Scattering from Natural Rough Surfaces Modeled by Fractional Brownian Motion Two-Dimensional Processes

Giorgio Franceschetti, *Fellow, IEEE*, Antonio Iodice, *Student Member, IEEE*, Maurizio Migliaccio, *Member, IEEE*, and Daniele Riccio, *Senior Member, IEEE*

***Abstract*—A model for electromagnetic scattering from natural rough surfaces described by means of fractional Brownian motion model is developed. The fractal surface model is employed to obtain the Kirchhoff solution of the Stratton–Chu scattering integral. An analytical viable formulation is achieved and compared to available classical solutions. Comparison with experimental data is also provided. Results show advantages of proposed solution from both theoretical and experimental viewpoint.**

***Index Terms*—Electromagnetic scattering by rough surfaces.**

I. Introduction and Motivations

THE problem of electromagnetic wave scattering from a randomly rough surface has been widely studied because of its great relevance in the fields of telecommunications and remote sensing. In the last decades, several approaches to the solution of this problem have been proposed and developed. Among them, the most popular ones are the Kirchhoff approach [1]–[3], the small perturbation method [2], [3], and the integral equation method [4], [5]: these approaches are based on different approximations and exhibit different ranges of validity [3], [5], [6]. In all cases, the surface is described by a stationary stochastic two-dimensional (2-D) process, with given probability density function (pdf) (usually Gaussian) and correlation function (usually Gaussian, exponential or combinations of these). Accordingly, the surface can be characterized by few parameters such as its height standard deviation σ and its correlation length L. The corresponding evaluated scattered fields are in excellent agreement with numerical simulations and laboratory measurements (performed by using artificial rough surfaces generated employing above surface models), while comparison with real data is less successful (see, e.g., [7]). This might be due to the presence of unmodeled volume scattering, but also to limitations of above surface model. In fact, measured natural surface height standard deviation and correlation length turn out to depend on the length of the considered profile [8] so that the process is not stationary.

Manuscript received February 13, 1998; revised March 17, 1999.

G. Franceschetti is with the Dipartimento di Ingegneria Elettronica, Università di Napoli Federico II, Napoli, 80125 Italy, and with the University of California, Los Angeles, CA 90024 USA.

A. Iodice and D. Riccio are with the Dipartimento di Ingegneria Elettronica, Università di Napoli Federico II, Napoli, 80125 Italy.

M. Migliaccio is with the Universitá di Cagliori, DIEE, Cagliori 09123, Italy.

Publisher Item Identifier S 0018-926X(99)07063-5.

In recent years it has been shown that a new description more suitable for natural rough surfaces, based on fractal geometry, can be conveniently used [9]. Effectiveness of fractal geometry for natural surface modeling was validated by generating surprisingly realistic synthetic terrain surfaces [9], [10]. More recently, field measurements have confirmed that soil surfaces show self-affinity properties on a wide range of scales [8] and that their spectra exhibit the shape $(1/f)^{\alpha}$ [8], [11]. For sea surfaces, $(1/f)^{\alpha}$ spectra are both obtained by field measurements and suggested by theoretical considerations [12]. All these results lead to describe natural surfaces by means of the fractional Brownian motion (fBm) fractal model [9], [13]. Therefore, there is an increasing consensus that it is of a great relevance to make use of this model for computation of scattering from natural surfaces.

Results of some studies on use of fractal surface models for the problem of electromagnetic wave scattering have recently been reported [12], [14]–[17]. All these studies employ the Kirchhoff approximation. In [12] and [14], attention is posed on normal incidence only; in [15]–[17] the fBm process is approximated by a Weierstrass–Mandelbrot bandlimited function. This latter approach has the advantage that an analytical expression (containing a few random parameters) of the surface is available. By varying some fractal parameters, different scattered field statistics actually observed in practice are obtained [16]. However, the final analytical expression of the scattered field is very involved and an analytical evaluation of its mean-square value is not available.

In this paper, we explore use of the fBm model with the Kirchhoff approach and the small-slope approximation, and we analytically evaluate in a closed form the mean-square value of the field scattered along an arbitrary direction by a surface illuminated by a plane wave. We obtain a general expression, which greatly simplifies in some special cases. Expression of the backscattering coefficient, i.e., of the normalized radar cross section, is also provided as a particular case. This allows to elucidate the dependence of the scattered field on the surface fractal parameters. A theoretical discussion on the validity of this model for the study of scattering from natural surfaces is carried out and, finally, some numerical examples are reported to compare obtained results to the ones of classical models and to some real data.

Before proceeding further, we stress that we do not use the fBm surface model for its mathematical convenience, but

because it best models natural rough surfaces (see [8]–[13]). Furthermore, it is important to elucidate the fact that the fBm fractal characterization exhibits some important advantages with respect to a generic power law description, which has sometimes been employed in literature, see e.g. [18]–[21]. First of all, fBm surface model is able to well describe the scale-invariance properties of natural surfaces [8]–[13] (see Section II). Another advantage of the fBm description, as shown in this paper, is related to the analytical evaluation of electromagnetic scattering. In fact, power law spectra are not easy to analytically handle within the Kirchhoff approach and numerical methods and/or Monte Carlo simulations are usually employed to evaluate the normalized radar cross section of a power law surface (see, for instance, [18]–[20]). In the following, we show that an analytical formulation of the normalized radar cross section can be obtained by using the fBm fractal characterization with no extra simplifying assumptions with reference to classical cases [21].

II. Surface Model

In this section, we describe and discuss the employed surface model. As already stated, we model natural surfaces by means of fBm 2-D processes.

A stochastic process $z(x,y)$ is an fBm surface if, for every x, y, x', and y', it satisfies the following relation [13]:

$$\Pr\{z(x,y)-z(x',y')<\bar{\zeta}\} = \frac{1}{\sqrt{2\pi}s\tau^H}\int_{-\infty}^{\bar{\zeta}}\exp\left(-\frac{\zeta^2}{2s^2\tau^{2H}}\right)d\zeta \tag{1}$$

where

$$\tau=\sqrt{(x-x')^2+(y-y')^2} \tag{2}$$

H is the Hurst coefficient and s is a real parameter measured in [m$^{(1-H)}$]. It can be demonstrated [13] that if $0<H<1$, a process satisfying (1) exists and that (with probability one) a fBm sample surface has a fractal dimension $D=3-H$. Furthermore, the parameter s is related to a characteristic length of the fBm surface called topothesy T [14], [12]

$$s=T^{(1-H)} \tag{3}$$

which is defined as the distance over which chords joining points on the surface have a root mean square (rms) slope equal to unity.

By using (3), (1) can be equivalently written as

$$\Pr\{z(x,y)-z(x',y')<\bar{\zeta}\} = \frac{1}{\sqrt{2\pi}T^{(1-H)}\tau^H}\int_{-\infty}^{\bar{\zeta}}\exp\left(-\frac{\zeta^2}{2T^{(2-2H)}\tau^{2H}}\right)d\zeta. \tag{4}$$

Besides, it can be shown that fBm surfaces are self affine, i.e., if we let $\Delta z(\tau)=z(x,y)-z(x',y')$, it turns out that for any $a>0$, $\Delta z(a\tau)$ has the same statistics as $a^H\Delta z(\tau)$. As a consequence, the ratio between vertical and horizontal surface variations (statistically) decreases as the considered scale length increases, except that for $H=1$.

It is important to note that the fBm process is nonstationary, but its increments over a fixed horizontal distance τ are stationary isotropic Gaussian processes with zero mean and variance equal to $T^{(2-2H)}\tau^{2H}$. This property allows the analytical evaluation of the backscattered power density, which is performed in the following sections. Due to stationarity of its increments, the structure function $D(\tau)\triangleq\langle|z(x,y)-z(x',y')|^2\rangle$ of an fBm process can be defined [22] and is equal to

$$D(\tau)=s^2\tau^{2H}=T^{(2-2H)}\tau^{2H}. \tag{5}$$

In the above relations, the symbol $\langle\cdot\rangle$ stands for statistical mean.

It can be also shown [11], [23] that the power spectrum of an fBm 2-D process is

$$S(\kappa)=S_0\kappa^{-\alpha} \tag{6}$$

wherein

$$\alpha=2+2H=8-2D \tag{7}$$

$$\kappa=\sqrt{\kappa_x^2+\kappa_y^2} \tag{8}$$

is the spatial frequency and S_0 is the spectral parameter ($S_0>0$).

We recall that structure function and power spectrum of an isotropic stochastic process with stationary increments are related by the following expression [22]:

$$D(\tau)=4\pi\int_0^\infty[1-J_0(\kappa\tau)]S(\kappa)\kappa\,d\kappa. \tag{9}$$

By using this expression, it is possible to find [12] the relation between s (5) and S_0 (6)

$$s^2=\frac{4S_0}{\alpha-2}\Gamma(3-\alpha)\sin\left(\frac{\pi}{2}(3-\alpha)\right)B\left(\frac{1}{2},\frac{\alpha-1}{2}\right) \tag{10}$$

wherein Γ and B are the Gamma and Beta functions [24], respectively.

Note that the power law spectrum of the fBm process has an exponent α [see (6)] which is limited to the interval $2<\alpha<4$, as can be verified from (7) by recalling that $0<H<1$. This explains the (otherwise "mysterious") fact that all measured soil surface spectra are power law ones with $\alpha\approx 3$ [8]–[10].

Finally, it is important to note that a surface satisfying (1) for every τ is self affine on all scales so that it has details on any arbitrarily small scale and is not differentiable in any point (although it is continuous). Therefore, Kirchhoff approximation, and more in general even the continuity conditions of tangential fields, cannot be used. We call such a surface a "mathematical" fBm surface [15]. However, natural surfaces have been shown to satisfy (1) only in a wide but limited range of scales $\tau_{\min}<\tau<\tau_{\max}$ or (see (6)] only in a wide but limited range of spatial frequencies $\kappa_{\min}<\kappa<\kappa_{\max}$. Besides, the range of scales of interest for our scattering problem is limited on one side by the finite dimension of the illuminated surface and on the other by the fact that surface

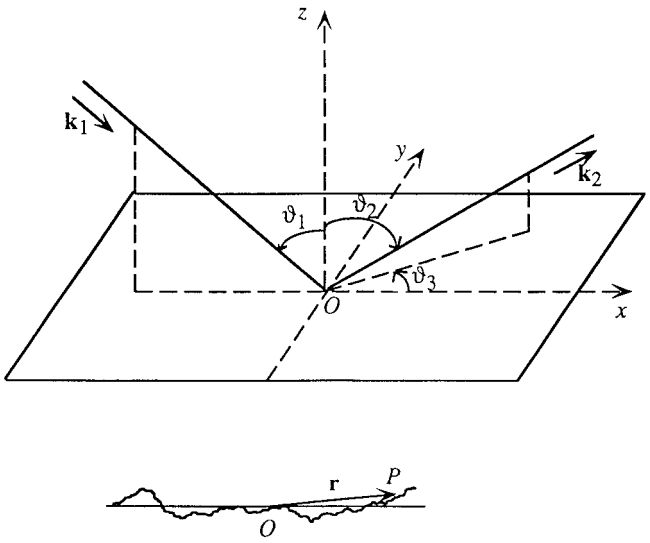

Fig. 1. Geometry of the problem.

variations on scales much smaller than wavelength do not affect the scattered field [16]. We refer as "physical" fBm surfaces [15] to those satisfying (1) only in a limited range of scales. For such surfaces, use of Kirchhoff approach and of small slope approximation is appropriate if some conditions on $\tau_{\min}, \tau_{\max}, T$ and H are satisfied (see Section IV) and if, at the smallest scales, the surface is sufficiently regular [12], [25].

III. Electromagnetic Scattering

A. General Case

In this section, we evaluate the mean-square value of the field scattered in an arbitrary direction by an fBm physical surface $z = z(x, y)$ illuminated by a plane wave. We follow the Kirchhoff approach and use the small slope approximation. A discussion on the validity of these approximations for real natural surfaces at microwave frequencies is addressed in the next section. Let

$$\hat{\mathbf{p}} E_p^{(i)} \exp(-j\mathbf{k}_1 \cdot \mathbf{r}) \tag{11}$$

the incident field (see Fig. 1), wherein p stands for h or v (horizontal or vertical polarization). Under the above mentioned hypotheses, the generic component of the scattered field (in the Fraunhofer region) is expressed by [2]

$$E_q^{(s)} = \frac{jk \exp(-jkR_0)}{4\pi R_0} E_p^{(i)} F_{pq}(\vartheta_1, \vartheta_2, \vartheta_3) \times \iint_A \exp(-j\mathbf{v} \cdot \mathbf{r})\, dA \tag{12}$$

where $\mathbf{v} = \mathbf{k_1} - \mathbf{k_2}$, i.e.,

$$\begin{cases} v_x = k(\sin\vartheta_1 - \sin\vartheta_2 \cos\vartheta_3) \\ v_y = -k \sin\vartheta_2 \sin\vartheta_3 \\ v_z = -k(\cos\vartheta_1 + \cos\vartheta_2). \end{cases} \tag{13}$$

In (11)–(13), $\mathbf{k}_1$ and $\mathbf{k}_2$ are the propagation vectors of the incident and scattered wave, respectively, k is the wavenumber, A is the area of the illuminated patch, and R_0 the distance from its center to the receiver, p and q can each stand for h or v, and the meaning of $\vartheta_1, \vartheta_2, \vartheta_3$ is illustrated in Fig. 1. In addition, $F_{pq}(\cdot)$ is a dimensionless function depending on the average Fresnel reflection coefficients over the mean plane, on the incidence and scattering angle and on the polarization. A detailed expression of the function F can be found in [2].

In Appendix A, we show how the use of (1) and (12) leads to the following expression of the mean-square value of the scattered field:

$$\left\langle \left| E_q^{(s)} \right|^2 \right\rangle = \frac{k^2 \left| E_p^{(i)} \right|^2 |F_{pq}|^2}{(4\pi R_0)^2} 2\pi A \frac{1}{2H} \sum_{n=0}^{\infty} \frac{(-1)^n v_{xy}^{2n}}{2^{2n}(n!)^2} \cdot \frac{\Gamma\left(\frac{n+1}{H}\right)}{\left(\frac{\sqrt{2}}{2}|v_z|s\right)^{\frac{2n+2}{H}}} \tag{14}$$

wherein $v_{xy} = \sqrt{v_x^2 + v_y^2}$.

Equation (14) can be rewritten in a more convenient form by using (3)

$$\left\langle \left| E_q^{(s)} \right|^2 \right\rangle = \frac{\left| E_p^{(i)} \right|^2 |F_{pq}|^2}{(4\pi R_0)^2} 2\pi A \frac{k^2 T^2}{2H} \sum_{n=0}^{\infty} \frac{(-1)^n (v_{xy} T)^{2n}}{2^{2n}(n!)^2} \cdot \frac{\Gamma\left(\frac{n+1}{H}\right)}{\left(\frac{\sqrt{2}}{2}|v_z|T\right)^{\frac{2n+2}{H}}}. \tag{15}$$

This expression shows more clearly that each term of the series is dimensionless.

Equations (14) or (15) hold for fBm physical surfaces satisfying (1) in a range of scales which includes the scale lengths appreciably affecting the scattered field (see Section IV and Appendix A). It is important to note that only the height increments of the surface are assumed to satisfy a stationary stochastic process and not the surface itself.

Equations (14) or (15) greatly simplify in the following three cases: scattering in the specular direction ($v_{xy} = 0$), Brownian surface ($H = 1/2$), and nonfractal surface ($H \to 1$).

B. Specular Direction

In the specular direction, we have $\vartheta_2 = \vartheta_1$ and $\vartheta_3 = 0$ (see Fig. 1), so that $v_x = v_y = v_{xy} = 0$ and $v_z = -2k\cos\vartheta_1$. Substituting these values in (15) we get

$$\left\langle \left| E_q^{(s)} \right|^2 \right\rangle = \frac{\left| E_p^{(i)} \right|^2 |F_{pq}|^2}{(4\pi R_0)^2} 2\pi A \frac{k^2 T^2}{2H} \cdot \frac{\Gamma\left(\frac{1}{H}\right)}{(\sqrt{2} k T \cos\vartheta_1)^{\frac{2}{H}}}. \tag{16}$$

C. Brownian Surface

A Brownian surface is obtained by setting $H = 1/2$ in (1). Its intersection with an arbitrary vertical plane is the graph of a Wiener process [13]. If we let $H = 1/2$ in (15), recalling the Taylor series expansion of the function $(1 + t^2)^{-3/2}$ we get

$$\left\langle \left| E_q^{(s)} \right|^2 \right\rangle = \frac{k^2 T^2 \left| E_p^{(i)} \right|^2 |F_{pq}|^2}{(4\pi R_0)^2} 2\pi A \times \frac{\frac{1}{2} v_z^2 T^2}{\left[\left(\frac{\sqrt{2}}{2} v_z T\right)^4 + (v_{xy} T)^2\right]^{3/2}}. \tag{17}$$

Equation (17) can be more easily obtained directly from (A.7) (see Appendix A) with $H = 1/2$ by using the relation [24]

$$\int_0^\infty J_0(b\tau)\exp(-u\tau)\tau\, d\tau = \frac{u}{(u^2+b^2)^{3/2}}. \tag{18}$$

D. Nonfractal Surface

The limiting case $H \to 1$ corresponds to a surface with fractal dimension equal to two, i.e., a regular (nonfractal) surface. In this case, the topothesy T has no meaning, while the parameter s becomes dimensionless and assumes the meaning of rms slope of the surface.

Substituting $H = 1$ in (14) and recalling the series expansion of the exponential function, we get

$$\left\langle \left|E_q^{(s)}\right|^2 \right\rangle = \frac{k^2\left|E_p^{(i)}\right|^2 |F_{pq}|^2}{(4\pi R_0)^2} 2\pi A \frac{1}{v_z^2 s^2}\exp\left(-\frac{v_{xy}^2}{2v_z^2 s^2}\right). \tag{19}$$

Equation (19) can be more easily obtained directly from (A.7) with $H = 1$ by using the relation [24]

$$\int_0^\infty J_0(b\tau)\exp(-u\tau^2)\tau\, d\tau = \frac{1}{2u}\exp\left(-\frac{b^2}{4u}\right). \tag{20}$$

It is interesting to note that (19) is coincident with the result obtained [1] in the case of very rough Gaussian surface with Gaussian correlation function.

E. Backscattering Coefficient

In order to simplify the discussion, in the next sections we refer to the backscattering coefficient (also referred to as surface normalized radar cross section), defined as [5]

$$\sigma_{pq}^0 = \frac{4\pi R_0^2 \left\langle \left|E_q^{(s)}\right|^2 \right\rangle}{A\left|E_p^{(i)}\right|^2} \tag{21}$$

when incidence and scattering directions coincide.

In the backscattering case, we have $\vartheta_2 = \vartheta_1$, $\vartheta_3 = \pi$, and hence (setting $\vartheta = \vartheta_1$)

$$\begin{cases} v_x = 2k\sin\vartheta \\ v_y = 0 \\ v_z = -2k\cos\vartheta \end{cases} \tag{22}$$

and it can be demonstrated that under the small slope approximation [2]

$$\begin{cases} F_{hh}(\vartheta) = -2R_h(\vartheta)\cos\vartheta \\ F_{hv}(\vartheta) = F_{vh}(\vartheta) = 0 \\ F_{vv}(\vartheta) = -2R_v(\vartheta)\cos\vartheta. \end{cases} \tag{23}$$

Then, use of (21)–(23) in (15) leads to

$$\sigma_{pp}^0 = \frac{|R_p(\vartheta)|^2 k^2 T^2 \cos^2\vartheta}{H}\sum_{n=0}^{\infty}\frac{(-1)^n (2kT\sin\vartheta)^{2n}}{2^{2n}(n!)^2} \cdot \frac{\Gamma\left(\frac{n+1}{H}\right)}{(\sqrt{2}kT\cos\vartheta)^{\frac{2n+2}{H}}}. \tag{24}$$

where $R(\vartheta)$ is the Fresnel reflection coefficient of the mean plane.

Scattering in the specular direction now occurs in the case of normal incidence. Substituting (21)–(23) in (16) we get

$$\sigma^0 = \frac{|R(0)|^2 k^2 T^2}{H}\cdot\frac{\Gamma\left(\frac{1}{H}\right)}{(\sqrt{2}kT)^{\frac{2}{H}}} \tag{25}$$

which, in the case of perfectly conducting surface, coincides with the expression found in [12].

For the Brownian surface (17), use of (21)–(23) leads to

$$\sigma_{pp}^0 = \frac{|R_p(\vartheta)|^2 (\sqrt{2}kT\cos\vartheta)^4}{[(\sqrt{2}kT\cos\vartheta)^4 + (2kT\sin\vartheta)^2]^{3/2}}. \tag{26}$$

Finally, for the nonfractal surface, we get

$$\sigma_{pp}^0 = \frac{|R_p(\vartheta)|^2}{2s^2}\exp\left(-\frac{\tan^2\vartheta}{2s^2}\right). \tag{27}$$

Few last words about the convergence rate of the series in (24). It decreases as the incidence angle increases and as kT decreases. In all the plots that we show (see Section V), a maximum of 100 terms was sufficient to ensure that the error on the backscattering coefficient was less than 0.1 dB.

IV. Validity of the Formulation

In order to have an idea of values assumed by fractal parameters for real natural surfaces, we recall some results available from literature. For natural soil surfaces, *in situ* measurements reported in [8] and [11] lead to fractal dimensions D larger than 2, but smaller than 2.5 (this corresponds to $0.5 < H < 1$) and to a spectral parameter S_0 ranging from 10^{-7} to 10^{-3} [m^{2-2H}] [i.e., see (2.10)] to a fractal parameter s^2 ranging from 10^{-6} to 10^{-1} [m^{2-2H}]. For example, on a rocky natural surface at Mt. St. Helens, a fractal dimension $D = 2.35$ $(H = 0.65)$ and a profile spectral parameter S_0 equal to 3.57×10^{-4} [m^{2-2H}] (by use of [11, eq. (51)) and of (10) and (3)], this corresponds to $s^2 = 2.8 \times 10^{-3}$ [m^{2-2H}] and $T = 2.25 \times 10^{-4}$ [m]) were found [11]. Besides, for this natural surface, (6) (i.e., "fBm-fractalness") turns out to hold for spatial frequencies ranging at least from 0.05 to 100 [m^{-1}] (i.e., scale lengths from less than 1 [cm] to more than 20 [m]).

With regard to sea surfaces, in [12] it is shown how a combination of theory and field measurements leads to $H = 0.75$ and $T = 1.3\times10^{-4}$ [m] (i.e., $s^2 = 1.14\times10^{-2}$ [m^{2-2H}]) for isotropic gravity waves in the equilibrium range with a friction velocity of 0.37 [m/s]. In this case, "fBm-fractalness" holds for scale lengths from a few centimeters to several meters [12].

We want now to verify that above mentioned ranges of scales include the scale lengths that appreciably contribute to scattering, so that calculations of Appendix A hold. Let us analyze the quantity

$$f(\tau) = \tau\exp[-2(ks\cos\vartheta)^2\tau^{2H}] \tag{28}$$

which appears in the argument of the integral of (A.7) for the backscattering case $(v_z = 2k\cos\vartheta)$. It can be easily

TABLE I
RANGE OF SCALES $[\bar{\tau}/10, 4\bar{\tau}]$ WHICH APPRECIABLY CONTRIBUTE TO SCATTERING FROM THE CONSIDERED SOIL SURFACE FOR DIFFERENT FREQUENCIES AND INCIDENCE ANGLE. SURFACE FRACTAL PARAMETERS: $D = 2.35$, $s^2 = 2.8 \times 10^{-3}$ [m^{2-2H}]. RANGE OF "fBm FRACTALNESS": FROM ABOUT 0.5 cm TO ABOUT 20 m

frequency \ incidence angle	ϑ=0°	ϑ=60°
500 MHz	0.12 - 4.8 [m]	0.36 - 14.0 [m]
1 GHz	0.04 - 1.6 [m]	0.12 - 4.8 [m]
5 GHz	0.0035 - 0.14 [m]	0.013 - 0.41 [m]

TABLE II
RANGE OF SCALES $[\bar{\tau}/10, 4\bar{\tau}]$ WHICH APPRECIABLY CONTRIBUTE TO SCATTERING FROM THE CONSIDERED SEA SURFACE FOR DIFFERENT FREQUENCIES AND INCIDENCE ANGLE. SURFACE FRACTAL PARAMETERS: $D = 2.25$, $s^2 = 1.14 \times 10^{-2}$ [m^{2-2H}]. RANGE OF "fBm FRACTALNESS": FROM ABOUT 1 cm TO SEVERAL METERS

frequency \ incidence angle	ϑ=0°	ϑ=60°
500 MHz	0.04 - 1.6 [m]	0.10 - 4.1 [m]
1 GHz	0.017 - 0.66 [m]	0.04 - 1.6 [m]
5 GHz	0.002 - 0.08 [m]	0.005 - 0.20 [m]

demonstrated that the function of (28) reaches its maximum for

$$\tau = \bar{\tau} = \left(\frac{1}{2ks\sqrt{H}\cos\vartheta}\right)^{\frac{1}{H}} = T\left(\frac{1}{2kT\sqrt{H}\cos\vartheta}\right)^{\frac{1}{H}}. \tag{29}$$

This point of maximum is proportional to $\lambda^{1/H}$. It can also be verified that if $H > 0.5$, the function in (28) is much smaller than its maximum for $\tau < \bar{\tau}/10$ and $\tau > 4\bar{\tau}$ and the contribution of these intervals to the integral of (A.7) is negligible. Therefore, only the scale lengths from $\bar{\tau}/10$ to $4\bar{\tau}$ appreciably contribute to scattering.

By inserting in (29) the fractal parameters of the soil surface analyzed in [11] and, considering three different frequencies (500 MHz, 1 GHz, 5 GHz), we obtain the intervals $[\bar{\tau}/10, 4\bar{\tau}]$ shown in Table I. They are all included in the interval of "fBm-fractalness."

By inserting in (29), the fractal parameters of the sea surface analyzed by [12] and considering the same three different frequencies, we obtain the intervals $[\bar{\tau}/10, 4\bar{\tau}]$ shown in Table II. Again, they are all included in the interval of "fBm-fractalness," except that at 5 GHz and small incidence angles.

As a summary of above results, we can state that usually, for the scale lengths of interest for microwave scattering, natural surfaces can be modeled as fractals, and that values of H ranging from 0.5 to 1 and values of s^2 of the order of 10^{-6}–10^{-1} [m^{2-2H}] are realistic ones.

At this point, a discussion on the range of validity of our model is in order. It is well known [2], [3], [5] that the Kirchhoff approximation holds if the surface mean radius of curvature is much greater than the wavelength and that the small slope approximation is valid if rms slope is much smaller than unity. However, radius of curvature and rms slope are not well defined for a "mathematical" fBm surface. For a "physical" fBm surface these quantities should be related to $\tau_{\min}$, $\tau_{\max}$, T, and H. The rigorous study of this point is beyond the scope of this paper and is matter of current study. A further discussion on this subject can be found in [25] and [26]. We want here only to show that a very simple condition for the validity of the small slope approximation can be obtained by the following heuristic considerations. It can be shown from (5) that the mean-square slope (MSS) of chords joining points at distance τ is

$$\left\langle \left| \frac{\Delta z(\tau)}{\tau} \right|^2 \right\rangle = T^{(2-2H)}\tau^{-(2-2H)}. \tag{30}$$

Therefore, this MSS increases as τ decreases and the maximum MSS is obtained for $\tau = \tau_{\min}$, where $\tau_{\min}$ is the smallest scale length which appreciably contributes to scattering. This maximum MSS is

$$\left\langle \left| \frac{\Delta z(\tau)}{\tau} \right|^2 \right\rangle_{\max} = T^{(2-2H)}\tau_{\min}^{-(2-2H)}. \tag{31}$$

If we want this MSS to be less than $1/10$ we get

$$\tau_{\min} \cong \frac{\bar{\tau}}{10} > 10^{\frac{1}{2-2H}}T. \tag{32}$$

By combining (29) and (32) we obtain

$$2kT\cos\vartheta < \frac{1}{\sqrt{H}\cdot 10^{H\frac{3-2H}{2-2H}}}. \tag{33}$$

It can be verified that natural surfaces considered at the beginning of this section satisfy this condition if the frequency is less than a few gigahertz.

V. NUMERICAL EXAMPLES AND COMPARISON WITH MEASUREMENTS

In this section, we present and discuss some examples aimed at studying the backscattering coefficient σ^0 evaluated by means of (24). In particular, we first of all examine the scattering dependence on the incidence angle ϑ, the Hurst coefficient H, the fractal parameter s^2, and the frequency f. This study is followed by a direct comparison of our model with some widespread scattering models and with a set of measured data.

In order to analyze the scattering dependence on the surface fractal parameters and on frequency, we show some results obtained inserting in (24) realistic fractal parameters. By considering results of the discussion of Section IV, we can state that usually, for the scale lengths of interest for microwave scattering, natural surfaces can be modeled as fractals and that values of H ranging from 0.5 to 1 and values of s^2 from 10^{-1} to 10^{-2} [m^{2-2H}] are realistic ones. Accordingly, we plot in Fig. 2 the backscattering coefficient at 1 GHz, hh polarization, as a function of the incidence angle ϑ for s^2 ranging from 0.04 to 0.10 [m^{2-2H}], $\varepsilon_r = 15$, and for (a) $H = 0.5$, (b) $H = 0.75$, and (c) $H = 1$. Plots of Fig. 2 clearly show that the dependence on the incidence angle is weakened by a decrease of H (i.e., an increase of the fractal dimension D) and by an increase of s^2. To better illustrate this point, in Fig. 3 we plot the backscattering coefficient versus H, Fig. 3(a), and

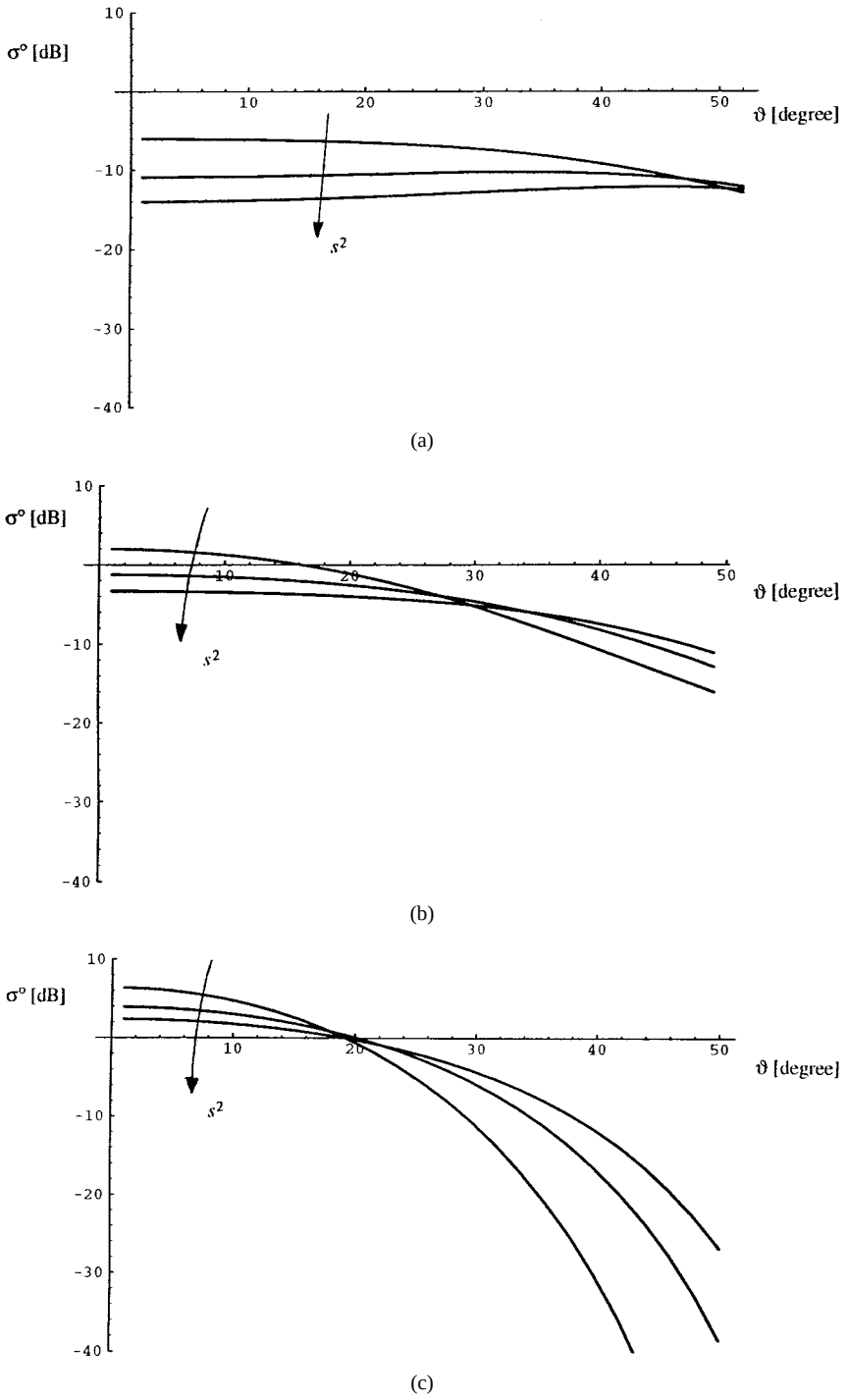

Fig. 2. Backscattering coefficient σ^0 at 1 GHz (hh polarization) as a function of the incidence angle for s^2 ranging from 0.04 to 0.10 [m^{2-2H}], $\varepsilon_r = 15$, and for (a) $H = 0.5$, (b) $H = 0.75$, and (c) $H = 1$.

versus s^2, Fig 3(b), for $\vartheta = 10°$ (long-dashed line), $\vartheta = 30°$ (solid line), $\vartheta = 50°$ (short-dashed line). The same frequency, polarization, and dielectric constant of Fig. 2 have been used. Analogous plots can be obtained for vv polarization. Plots of Fig. 3 show that at low-incidence angles the backscattered field decreases as D and s^2 increase, while at high incidence angles the backscattered field increases with D and s^2. This is in agreement with intuition since a higher fractal dimension D corresponds to a rougher surface and the parameters s is in some way related to the surface slope.

Examination of (24)–(27) shows that scattering by a fractal surface is frequency dependent; this dependence becomes weaker as H approaches unity and scattering becomes frequency independent when $H = 1$. To emphasise this point, we plot in Fig. 4 the backscattering coefficient as a function of frequency, at (a) $\vartheta = 10°$, (b) $\vartheta = 30°$, (c) $\vartheta = 50°$, hh polarization, for s^2 equal to 0.07 [m^{2-2H}], $\varepsilon_r = 15$, and for $H = 0.5$ (long-dashed line), $H = 0.75$ (solid line), and $H = 1$ (short-dashed line). These plots clearly show that for $H = 1$ scattering is frequency independent while, for $H < 1$, at

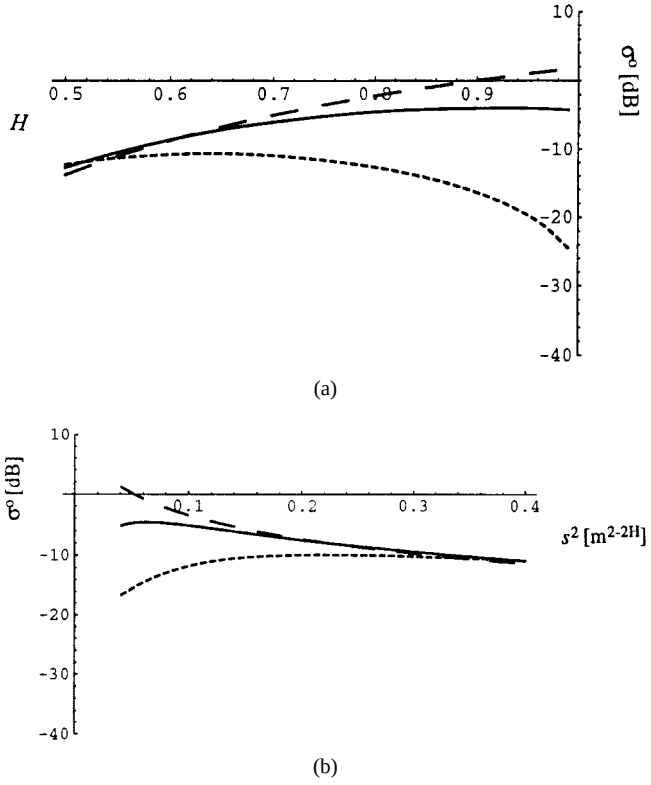

Fig. 3. Backscattering coefficient σ^0 versus (a) H and versus (b) s^2 for $\vartheta = 10°$ (long-dashed line), $\vartheta = 30°$ (solid line), $\vartheta = 50°$ (short-dashed line), at 1 and 5 GHz, hh polarization, $\varepsilon_r = 15$. In (a) $s^2 = 0.10$ [m^{2-2H}] and in (b) $H = 0.75$.

low and intermediate incidence angles, the backscattered field decreases as frequency increases. At higher incidence angles ($\vartheta = 50°$), for $H = 0.5$ the backscattered field still decreases with frequency, but with a smaller rate, and for $H = 0.75$ it increases with frequency. This behavior can be explained by considering that at higher frequencies smaller scale lengths are involved in the scattering, and that at smaller scales the ratio between vertical and horizontal surface variations increases (see Section II), so that a rougher surface is "seen" by the incident wave.

Let us now move to a direct comparison of our model with some measured data that can be found in literature. We also compare our fractal model with the Gaussian surface height model with Gaussian and exponential correlations, which, as in our case, obtain a scattering formulation in a closed-form[1] [2], [3]

$$\sigma^0_{pp} = |R_p(\vartheta)|^2 \cdot 2k^2 \cos^2\vartheta \cdot \exp[-(2k\sigma\cos\vartheta)^2] \times \sum_{n=1}^{\infty} \frac{(2k\sigma\cos\vartheta)^{2n}}{n!} \cdot W^{(n)}(2k\sin\vartheta). \quad (34)$$

Equation (34) is valid in the Kirchhoff and small slope approximation and the function $W^{(n)}(\cdot)$ is the Fourier transform of the nth power of the surface correlation function

$$W^{(n)}(2k\sin\vartheta) = \frac{L^2}{2n}\exp\left[-\frac{(2kL\sin\vartheta)^2}{4n}\right] \quad (35)$$

[1]For other correlation functions, a numerical integration is needed to evaluate the functions $W^{(n)}$.

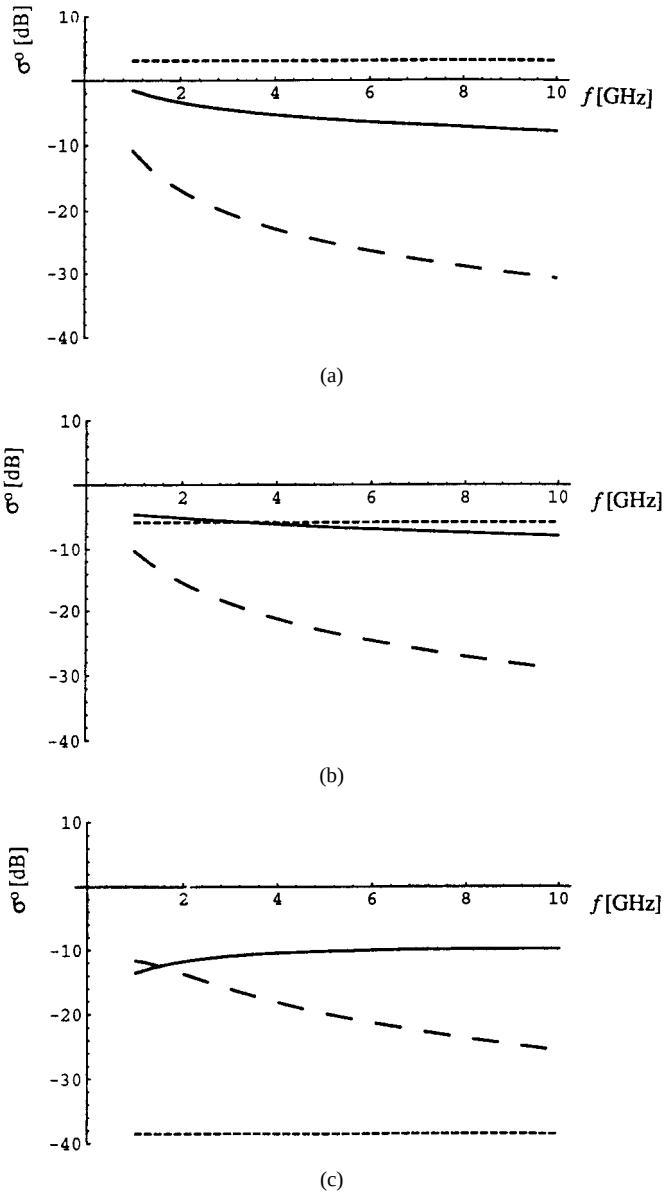

Fig. 4. Backscattering coefficient σ^0 as a function of frequency, at (a) $\vartheta = 10°$, (b) $\vartheta = 30°$, (c) $\vartheta = 50°$, hh polarization for s^2 equal to 0.07 [m^{2-2H}], $\varepsilon_r = 15$, and for $H = 0.5$ (long-dashed line), $H = 0.75$ (solid line), and $H = 1$ (short-dashed line).

for a Gaussian correlation function and

$$W^{(n)}(2k\sin\vartheta) = \frac{L^2}{n^2}\left[1 + \frac{(2kL\sin\vartheta)^2}{n^2}\right]^{-1.5} \quad (36)$$

for an exponential correlation function. In (34)–(36) σ and L are the surface height standard deviation and correlation length, respectively.

In the plots of Fig. 5, the case (reported in [7]) of a bare soil surface, whose characteristic parameters are summarized in Table III (surface A), is considered. Measured scattering coefficient data at L, C, and X bands are taken from [4] and [7]. In Fig. 5 the measured data are represented by dots; the scattering model relying on the fBm fractal surface model is represented by the solid line whereas the scattering model relying on the Gaussian surface model with Gaussian and exponential correlation functions are plotted for reference with

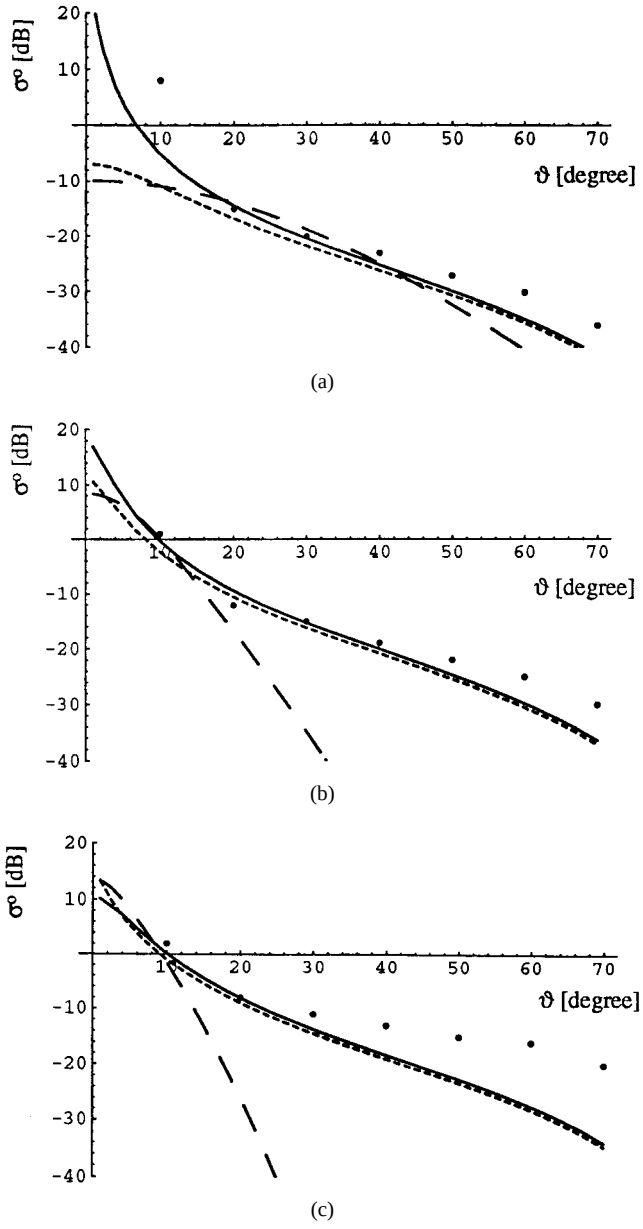

Fig. 5. Surface A backscattering coefficient σ^0 hh polarization at (a) 1.5 GHz, (b) 4.75 GHz, and (c) 9.5 GHz, as a function of the incidence angle: measured data (dots), fBm (solid line), Gaussian correlation (long-dashed line), exponential correlation (short-dashed line). Surface parameters are reported in Table III.

dashed lines. The long-dashed line is relevant to the Gaussian correlation function, the short-dashed line is relevant to the exponential correlation function. The same format is employed in all subsequent figures. In Fig. 5(a)–(c), the L-band (1.5 GHz), C-band (4.75 GHz), and X-band (9.5 GHz) cases are shown, respectively; hh polarization is considered. The model data fitting has been tentatively obtained for the fBm model[2] by using a least-square method.

The following comments are in order. First of all, the Gaussian correlation model is not in good agreement with measured data; besides, the exponential correlation model and the fBm (with $H = 0.5$, $s^2 = 4.5$, 10^{-4} [m^{2-2H}]) generally

[2]Data fitting applied to the other models did not improve presented results based on measured surface parameters.

TABLE III
CHARACTERISTIC PARAMETERS OF THE NATURAL SURFACES CONSIDERED IN FIGS. 5–7. PERMITTIVITY ε_r AND CLASSICAL SURFACE PARAMETERS σ AND L ARE TAKEN FROM [7] AND [3]. FRACTAL PARAMETERS H AND s^2 HAVE BEEN OBTAINED BY FITTING DATA WITH OUR MODEL

Surface	ε_r	σ [cm]	L [cm]	H	s^2 [m^{2-2H}]
A (Fig.5)	L-band 8.0–j2.0 C-band 8.8–j1.0 X-band 5.7–j1.3	0.40	8.4	0.5	$4.5\ 10^{-4}$
B (Fig.6)	$19 - j2.0$	2.6	20.3	0.58	$9.5\ 10^{-3}$
C (Fig.7)	$19 - j2.0$	4.3	38.7	0.95	0.1

provide similar results in good agreement with measurements. This is not true for large incident angles at X-band and for small incident angles at L-band. In the first case, both models fail [see Fig. 5(c)], most likely because multiple scattering and shadowing effects are not considered. Conversely, in the second case [see Fig. 5(a)], the fBm model provides a much better agreement with real data. Therefore, we can state that for the considered data set, the overall behavior of the scattering model based on fBm surface description is superior to the one based on classical surface descriptions. In order to obtain a more quantitative comparison, we evaluate the rms difference Δ between each model results and measured data

$$\Delta = \sqrt{\frac{\sum_{i=1}^{N} \left(\sigma^0_{\mathrm{dB}\,i} - \sigma^0_{\mathrm{dB}\,i\,\mathrm{meas}}\right)^2}{N}} \tag{37}$$

where N is the number of measured data points. We get $\Delta = 5.9$ dB for fBm, $\Delta = 7.0$ dB for exponential correlation, and $\Delta = 68.9$ dB for Gaussian correlation.

Let us now move to a different measurement data set. The case reported in [3, p. 992] is considered. The soil surface parameters are summarized in Table III (surface B), whereas the frequency is 2.25 GHz and polarization is vv. Corresponding measured and calculated backscattering coefficients are plotted in Fig. 6. Again, exponential correlation and fBm (with $H = 0.58$, $s^2 = 0.95$, 10^{-2} [m^{2-2H}]) models are in much better agreement with measured data than Gaussian correlation model and fBm model provides slightly better results than exponential correlation, especially at near vertical incidence. In this case, we get $\Delta = 1.05$ dB for fBm, $\Delta = 1.97$ dB for exponential correlation, and $\Delta = 4.14$ dB for Gaussian correlation.

Finally, let us consider another natural soil surface, also reported in [3], whose parameters are summarized in Table III (surface C). As in the previous case, frequency is 2.25 GHz and polarization is vv. Corresponding measured and calculated backscattering coefficients are plotted in Fig. 7. These plots clearly show that in this case fBm model (with $H = 0.95$, $s^2 = 0.1$ [m^{2-2H}]) provides the best agreement with measured data among the considered models. In fact, we get $\Delta = 0.58$ dB for fBm, $\Delta = 2.24$ dB for exponential correlation, and $\Delta = 5.56$ dB for Gaussian correlation.

As a summary of above results, we can state that our model provides scattering estimates, which can significantly differ

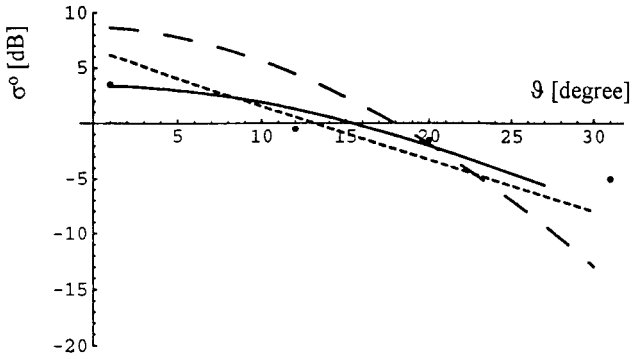

Fig. 6. Surface B backscattering coefficient σ^0 at 2.25 GHz, vv polarization, as a function of the incidence angle: measured data (dots), fBm (solid line), gaussian correlation (long-dashed line), exponential correlation (short-dashed line). Surface parameters are reported in Table III.

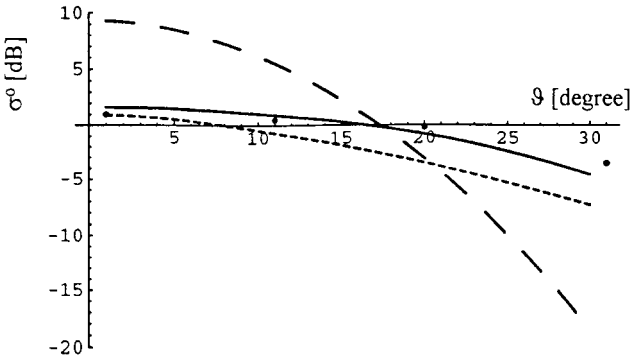

Fig. 7. Surface C backscattering coefficient σ^0 at 2.25 GHz, vv polarization as a function of the incidence angle: measured data (dots), fBm (solid line), Gaussian correlation (long-dashed line), exponential correlation (short-dashed line). Surface parameters are reported in Table III.

from the ones obtained by more classical models and which are always in better or comparable agreement with measured data considered here. This encourages further testing of our model. In particular, it must be noted that fractal parameters of previously considered surfaces are not known, but have been obtained by fitting measured scattering coefficients with our model. A comparison with measured scattered fields relevant to natural surface with known fractal parameters would be highly desirable. Unfortunately, such data are not available at present. Therefore, we believe that, as a guideline for future work, it is advisable to collect scattered data over surfaces whose fractal parameters have been measured or vice-versa to measure fractal parameters of surfaces for which scattered field data are available.

VI. Conclusion

The fBm fractal model has been shown to be particularly suitable for the description of natural surfaces. In this paper, we have shown that by using the Kirchhoff approach and the small slope approximation, it is possible to analytically evaluate the mean-square value of the field scattered by a natural surface described by the fBm fractal model. This possibility is basically due to the fact that fBm surface increments over a fixed distance are stationary. We have thus obtained a general formulation that greatly simplifies in some relevant particular cases. The expression of the backscattering coefficient has been also derived.

As expected, the backscattered field dependence on the incidence angle is weakened by an increase of the fractal dimension D and/or of s^2. Besides, the scattering turns out to be frequency dependent, except that for $D \to 2$.

It must be stressed how the suggested method requires a minimal amount of assumptions on the surface since only the process $(z_1 - z_2)$ must be specified. The price to be paid is that only second-order statistical parameter, i.e., the scattered power density, can be obtained. This is sufficient in most remote sensing application (see, for instance, [2], [3], and [5]). As a matter of fact, the surface scattering coefficient, i.e., the normalized radar cross section can be determined [see (21)]. By its knowledge, important information can be extracted about the surface electromagnetic and geometric properties (see [3], [5], and [7]). In any case, when it is important to have a closed-form expression of the complex scattered field, the approach that we proposed in [16] or other approaches also based on the Weierstrass–Mandelbrot function [15], [17] can be used. However, we stress again that with those approaches a closed-form expression of the mean-square value of the scattered field cannot be obtained, and statistics (and mean-squared value) of the scattered field must be measured by performing a Monte Carlo simulation [16].

A theoretical discussion on the validity of our model for the scattering from natural surfaces has been also carried out. In particular, we have verified that most natural surfaces studied in literature can indeed be modeled as fractals in a wide range of scales including scale lengths of interest for microwave scattering and that for these surfaces and frequencies, the small slope approximation can be used.

Finally, a comparison with measured data has been performed. It shows that our model results are in good agreement with measurements with a superior (or comparable) fitting compared to the use of more classical ones.

It can be concluded that use of fBm fractal surface model for the evaluation of electromagnetic scattering from natural surfaces is viable and effective, and that it is worthwhile exploring further this subject.

A few last words on future possible applications of our model in practical situations are in order. First of all, note that although the full definition of an algorithm for the estimation of the model parameters is certainly beyond the scope of our paper, the fitting procedure cited in Section V can be itself a (rough) method for parameters estimation. Furthermore, fractal surface parameters provide important information on the surface state and shape and, therefore, they can be used for characterization and classification purposes, possibly in conjunction with other more conventional parameters [27]–[29].

Appendix A

In this Appendix the analytical evaluation of the mean-square value of the scattered field is detailed.

Equation (12) can be more explicitly written as

$$E_q^{(s)} = \frac{jk\exp(-jkR_0)}{4\pi R_0} E_p^{(i)} F_{pq}(\vartheta_1,\vartheta_2,\vartheta_3) \times \iint_A \exp[-j(v_x x + v_y y + v_z z(x,y))]\,dx\,dy. \tag{A.1}$$

Taking the mean-square value we get

$$\left\langle \left|E_q^{(s)}\right|^2 \right\rangle = \frac{k^2 \left|E_p^{(i)}\right|^2 |F_{pq}|^2}{(4\pi R_0)^2} \iiint\!\!\iint \exp[-jv_x(x-x') - jv_y(y-y')] \langle \exp[-jv_z(z-z')] \rangle\,dx\,dx'\,dy\,dy' \tag{A.2}$$

where $z = z(x,y)$, $z' = z(x',y')$.

Note that $\langle \exp[-jv_z(z-z')] \rangle$ is the characteristic function of $z - z'$. Use of (1) leads to

$$\langle \exp[-jv_z(z-z')] \rangle = \exp\left[-\frac{1}{2}v_z^2 D(\tau)\right] = \exp\left[-\frac{1}{2}v_z^2 s^2 \tau^{2H}\right]. \tag{A.3}$$

By using this relation, performing the following coordinate transformation:

$$\begin{cases} x - x' = \tau\cos\varphi \\ y - y' = \tau\sin\varphi \\ x = x \\ y = y \end{cases} \tag{A.4}$$

and integrating over x and y, (A.2) becomes

$$\left\langle \left|E_q^{(s)}\right|^2 \right\rangle = \frac{k^2 \left|E_p^{(i)}\right|^2 |F_{pq}|^2}{(4\pi R_0)^2} A \iint \exp[-j(\tau v_x\cos\varphi + \tau v_y \sin\varphi)] \exp\left[-\frac{1}{2}v_z^2 s^2 \tau^{2H}\right] \tau\,d\varphi\,d\tau. \tag{A.5}$$

In (A.5), integration is extended to the whole plane. This is possible if the linear size l of the illuminated patch is such that

$$v_z s l^H \gg 1. \tag{A.6}$$

In fact, this condition ensures that the argument of the integral is negligible outside the original integration domain.

Integration of (A.5) over φ leads to [24]

$$\left\langle \left|E_q^{(s)}\right|^2 \right\rangle = \frac{k^2 \left|E_p^{(i)}\right|^2 |F_{pq}|^2}{(4\pi R_0)^2} 2\pi A \int_0^\infty J_0(v_{xy}\tau) \times \exp\left[-\frac{1}{2}v_z^2 s^2 \tau^{2H}\right] \tau\,d\tau \tag{A.7}$$

wherein $v_{xy} = \sqrt{v_x^2 + v_y^2}$. From the series expansion of the zero order Bessel function [24]

$$J_0(t) = \sum_{n=0}^{\infty} (-1)^n \frac{t^{2n}}{2^{2n}(n!)^2} \tag{A.8}$$

and the relation [24]

$$\int_0^\infty \exp(-u\tau^v)\cdot\tau^w\,d\tau = \frac{1}{v}\cdot\frac{1}{u^{\frac{w+1}{v}}}\cdot\Gamma\left(\frac{w+1}{v}\right) \quad \mathrm{Re}(u)>0,\quad \mathrm{Re}(v)>0,\quad \mathrm{Re}(w)>-1 \tag{A.9}$$

we get

$$\int_0^\infty J_0(b\tau)\exp(-u\tau^v)\tau\,d\tau = \sum_{n=0}^{\infty}\frac{(-1)^n b^{2n}}{2^{2n}(n!)^2}\int_0^\infty \exp(-u\tau^v)\tau^{2n+1}\,d\tau = \frac{1}{v}\sum_{n=0}^{\infty}\frac{(-1)^n b^{2n}}{2^{2n}(n!)^2}\cdot\frac{\Gamma\left(\frac{2n+2}{v}\right)}{u^{\frac{2n+2}{v}}}. \tag{A.10}$$

Specifying this relation with $u = v_z^2 s^2/2$, $b = v_{xy}$, and $v = 2H$, (A.7) becomes

$$\left\langle \left|E_q^{(s)}\right|^2 \right\rangle = \frac{k^2 \left|E_p^{(i)}\right|^2 |F_{pq}|^2}{(4\pi R_0)^2} 2\pi A \frac{1}{2H}\sum_{n=0}^{\infty}\frac{(-1)^n v_{xy}^{2n}}{2^{2n}(n!)^2} \cdot \frac{\Gamma\left(\frac{n+1}{H}\right)}{\left(\frac{\sqrt{2}}{2}|v_z|s\right)^{\frac{2n+2}{H}}}. \tag{A.11}$$

As a last remark, note that the integral of (A.7) spans all the τ interval from zero to ∞, while natural surfaces are described by a wide but limited range of τ values (see Sections II and IV). However, outside this interval, the value of the integrand is usually negligible (see Section IV) and its relevance to the integral can be ignored.

REFERENCES

[1] P. Beckmann and A. Spizzichino, *The Scattering of Electromagnetic Waves from Rough Surfaces*. Norwood, MA: Artech House, 1987.

[2] L. Tsang, J. A. Kong, and R. T. Shin, *Theory of Microwave Remote Sensing*. New York: Wiley, 1985.

[3] F. T. Ulaby, R. K. Moore, and A. K. Fung, *Microwave Remote Sensing*. Reading, MA: Addison-Wesley, 1982, vol. II.

[4] A. K. Fung, Z. Li, and K. S. Chen, "Backscattering from a randomly rough dielectric surface," *IEEE Trans. Geosci. Remote Sensing*, vol. 30, pp. 356–369, Mar. 1992.

[5] A. K. Fung, *Microwave Scattering and Emission. Models and Their Applications*. Norwood, MA: Artech House, 1994.

[6] M. F. Chew and A. K. Fung, "A numerical study of the regions of validity of the Kirchhoff and small-perturbation rough surface scattering models," *Radio Sci.*, vol. 23, no. 2, pp. 163–170, Mar./Apr. 1988.

[7] Y. Oh, K. Sarabandi, and F. T. Ulaby, "An empirical model and an inversion technique for radar scattering from bare soil surfaces," *IEEE Trans. Geosci. Remote Sensing*, vol. 30, pp. 370–381, Mar. 1992.

[8] S. R. Brown and C. H. Scholz, "Broad-band study of the topography of natural rock surfaces," *J. Geophys. Res.*, vol. 90, no. B14, pp. 12575–12582, Dec. 1985.

[9] B. B. Mandelbrot, *The Fractal Geometry of Nature*. New York: Freeman, 1983.

[10] R. F. Voss, "Random fractal forgeries," in *Fundamental Algorithms for Computer Graphics*, R. A. Earnshaw, Ed. Berlin, Germany: Springer-Verlag, 1985, pp. 805–835.

[11] T. R. Austin, A. W. England, and G. H. Wakefield, "Special problems in the estimation of power-law spectra as applied to topographical modeling," *IEEE Trans. Geosci. Remote Sensing*, vol. 32, pp. 928–939, July 1994.

[12] Y. Agnon and M. Stiassnie, "Remote sensing of the roughness of a fractal sea surface," *J. Geophys. Res.*, vol. 96, no. C7, pp. 12773–12779, July 1991.

[13] K. Falconer, *Fractal Geometry*. Chichester, U.K.: Wiley, 1990.

[14] M. V. Berry and T. M. Blackwell, "Diffractal echoes," *J. Phys. A Math. Gen.*, vol. 14, pp. 3101–3110, 1981.

[15] D. L. Jaggard, "On fractal electrodynamics," in *Recent Advances in Electromagnetic Theory*, H. N. Kritikos and D. L. Jaggard, Eds. Berlin, Germany: Springer-Verlag, 1990, pp. 183–223.

[16] G. Franceschetti, M. Migliaccio, and D. Riccio, "An electromagnetic fractal-based model for the study of fading," *Radio Sci.*, vol. 31, pp. 1749–1759, Nov./Dec. 1996.

[17] J. Chen, T. K. L. Lo, H. Leung, and J. Litva, "The use of fractals for modeling EM waves scattering from rough sea surface," *IEEE Trans. Geosci. Remote Sensing*, vol. 34, pp. 966–972, July 1996.

[18] E. Bahar, D. E. Barrick, and M. A. Fitzwater, "Computations of scattering cross sections for composite surfaces and the specification of the wavenumber where spectral splitting occurs," *IEEE Trans. Antennas Propagat.*, vol. AP-31, pp. 698–709, Sept. 1983.
[19] J. C. West, B. S. O'Leary, and J. Klinke, "Numerical calculation of electromagnetic scattering from measured wind-roughned water surfaces," *Int. J. Remote Sensing*, vol. 19, no. 7, pp. 1377–1393, 1998.
[20] H. T. Chou and J. T. Johnson, "A novel acceleration algorithm for the computation of scattering from rough surfaces with the forward-backward method," *Radio Sci.*, vol. 33, pp. 1277–1287, Sept./Oct. 1998.
[21] E. Rodriguez, "Beyond the Kirchhoff approximation," *Radio Sci.*, vol. 24, pp. 681–693, Sept./Oct. 1989.
[22] A. Ishimaru, *Wave Propagation and Scattering in Random Media*. New York: Academic, 1993.
[23] P. Flandrin, "On the spectrum of fractional Brownian motions," *IEEE Trans. Inform. Theory*, vol. 35, pp. 197–199, Jan. 1989.
[24] I. S. Gradshteyn and I. M. Ryzhik, *Table of Integrals, Series, and Products*. New York: Academic, 1980.
[25] R. E. Glazman, "Near-nadir radar backscatter from a well developed sea," *Radio Sci.* vol. 25, pp. 1211–1219, 1990.
[26] A. Collaro, G. Franceschetti, M. Migliaccio, and D. Riccio, "Gaussian rough surfaces and Kirchhoff approximation," *IEEE Trans. Antennas Propagat.*, to be published
[27] K. Yocoya, K. Yamamoto, and N. Funakubo, "Fractal-based analysis and interpolation of 3D natural surface shapes and their application to terrain modeling," *Computer Vision, Graphics, Image Processing*, vol. 46, pp. 284–302, 1989.
[28] C. V. Stewart, B. Moghaddam, K. J. Hintz, and L. M. Novak, "Fractional Brownian motion models for synthetic aperture radar imagery scene segmentation," *Proc. IEEE*, vol. 81, pp. 1511–1522, 1993.
[29] M. Coltelli, G. Fornaro, G. Franceschetti, R. Lanari, M. Migliaccio, J. R. Moreira, K. P. Papathanassiou, G. Puglisi, D. Riccio, and M. Schwäbisch, "SIR-C/X-SAR multifrequency multipass interferometry: A new tool for geological interpretation," *J. Geophys. Res.*, vol. 101, pp. 23127–23148, 1996.

Giorgio Franceschetti (S'60–M'62–SM'85–F'88), for a photograph and biography, see this issue, p. 1404.

Antonio Iodice (S'97) was born in Naples, Italy, on July 4, 1968. He received the Laurea degree in electronic engineering and the Ph.D. degree in electronic engineering and computer science, both from the University of Naples "Federico II", Naples, Italy, in 1993 and 1999, respectively.

He is currently with the Department of Electronic and Telecommunication Engineering, University of Naples "Federico II". His main research interests are in the field of Synthetic Aperture Radar (SAR) remote sensing: modeling of electromagnetic scattering from natural surfaces and SAR interferometry.

Dr. Iodice received a grant in 1995 from CNR (Italian National Council of Research) to be spent at IRECE (Istituto di Ricerca per l'Elettromagnetismo e i Componenti Elettronici), Naples, Italy, for research in the field of remote sensing.

Maurizio Migliaccio (M'90) was born in Naples, Italy. He received the Laurea degree (*summa cum laude*) in electronic engineering from the Università di Napoli "Federico II," Naples, Italy, in 1987.

He joined the Department of Electronic Engineering (Electromagnetic Division), Università di Napoli "Federico II," in 1987. In 1990 he became a University Researcher at the Istituto Universitario Navale (IUN), Naples, Italy, where he joined the Electromagnetic Waves Institute. Since 1993 he has taught microwave remote sensing at the IUN. In 1998 he became an Associate Professor at the Universitá di Cagliari, Sardinia, Italy, where he teaches microwave remote sensing. In 1993, 1998, and 1999 he has been an Adjoint Scientific Researcher in the Italian National Council of Research (CNR)—IRECE in the remote sensing field. He has been participating in an International NASA-ASI-DARA project on interferometry. He has been Visiting Scientist at the DLR (German Aerospace Agency), Oberpfaffenhofen, Germany. His main research activities have included active microwave remote sensing, electromagnetic modeling and natural scenes, electromagnetic fractal modeling, stochastic electromagnetic fields sampling, and electromagnetic reverberating chambers.

Mr. Migliaccio has been member of the IUN AdCom and was European Union Secretary of the COST 243 project on electromagnetic compatibility. He is member of the AGU.

Daniele Riccio (M'91–SM'99) was born in Naples, Italy, on April 13, 1962. He received the Laurea degree in electronic engineering from the University of Naples "Federico II," Italy, in 1989.

He was a Research Scientist at the "Istituto di Ricerca sull'Elettromagnetismo e i Componenti Elettronici" (IRECE) of the Italian National Council of Research (CNR). Since 1994 he has been a Research Scientist at the Department of Electronic and Telecommunication Engineering, University of Naples "Federico II," Italy, where he is a Lecturer of remote sensing and electromagnetic diagnostic. In 1994 and 1995 he was also a Guest Scientist at the DLR (German Aerospace Agency), Oberpfaffenhofen, Germany. Since 1998 he has also been a Research Scientist at IRECE. His main research activities are in the fields of simulation and modeling of synthetic aperture radar signals relevant to terrestrial and oceanic scenes, as well as in the application of fractal geometry to electromagnetic scattering and remote sensing.

Mr. Riccio won several fellowships from private and public companies (SIP, Selenia, CNR, CORISTA, CRATI) for research in the remote sensing field.